Effects of Viscosity and Modes on Transonic Aerodynamic and Aeroelastic Characteristics of Wings

Guru P. Guruswamy*
NASA Ames Research Center, Moffett Field, California

John W. Marstiller† and Henry T. Y. Yang‡
Purdue University, West Lafayette, Indiana
and
Peter M. Goorjian§
NASA Ames Research Center, Moffett Field, California

The research reported in this paper is concerned with aerodynamic and aeroelastic computations in the transonic regime. The aerodynamic computations were made using small-disturbance, unsteady, transonic theory with viscous corrections. Areas of investigation included studying the effects of viscous corrections on the aerodynamics about wings and the effect of including higher structural modes in addition to the fundamental bending and torsion modes in transonic aeroelastic analyses. Two wings were studied, a rectangular wing, with a NACA 64A010 airfoil section, and a swept wing, with an MBB-A3 supercritical airfoil section. Viscous effects on both wings were analyzed by employing the viscous wedge and lag-entrainment methods. Aeroelastic analyses were performed, and the effects of including the first two bending and torsion modes into the analysis are shown. Also discussed are the practical aspects of generating unsteady, transonic aerodynamic coefficients. Results from this work show that the inclusion of viscous effects increases the flutter speed for the two wings studied. For the rectangular wing, the fundamental modes were sufficient to determine the flutter speed, but the second torsion mode was required for an accurate aeroelastic analysis of the swept wing. These studies can aid aeroelasticians in selecting viscous methods and also structural modes to conduct aeroelastic analyses in the transonic regime.

Introduction

EXTENSIVE research in the area of two-dimensional, unsteady, transonic aerodynamics, as well as advancements in computer storage and efficiency, have recently allowed the practical computation of three-dimensional, unsteady, transonic airloads. Several methods have been considered for these computations. Traci et al.[1] developed the codes TDSTRN and TDUTRN to compute steady and unsteady transonic airloads, using the harmonic method. Borland et al.[2] developed a three-dimensional, unsteady, small-disturbance, transonic code, XTRAN3S, which is based on a time-integration method. This code is being evaluated by several groups and is used to calculate the aerodynamics in this study. Only limited aeroelastic analyses have been made using XTRAN3S. Borland and Rizzetta[3] determined the flutter speed vs Mach number for an unswept rectangular wing using the time-response method contained in XTRAN3S. Guruswamy and Goorjian[4] found the transonic flutter speed for an unswept rectangular wing, and Myers et al.[5] determined the flutter speed for a transport wing. In Refs. 4 and 5, XTRAN3S was used to compute the airloads in a three-dimensional, inviscid flowfield. To date, no three-dimensional aeroelastic analyses have been performed that have included the effects of flow viscosity.

Viscosity can play an important role in both the aerodynamic and aeroelastic characteristics of wings, as indicated by Guruswamy and Goorjian[6] who used the two-dimensional code LTRAN2 (viscous) to study airfoils. In transonic flow, viscous effects can alter the shock location and strength. These changes in the pressure distribution along the chord will also influence the aeroelastic characteristics of the wing. The XTRAN3S code has been upgraded, to include the effects of flow viscosity, by Rizzetta and Borland.[7] Two models are used to account for the viscous effects in XTRAN3S: The viscous wedge is an empirical method, and the lag-entrainment method is based on a set of integral boundary-layer equations. Computing time would increase considerably if more exact equations, such as the Navier-Stokes equations, were used to calculate the three-dimensional viscous effects. These methods are the same as those first incorporated into LTRAN2 (viscous).[6] The same viscous equations used in two dimensions are applied stripwise along the span to yield a three-dimensional correction. In this work, studies were made to determine the influence of viscous effects on the aerodynamic and aeroelastic characteristics of wings in transonic flow, using both methods.

It is important to study the structural modes to determine which are significant to the aeroelastic analysis. The deflection of an oscillating wing is exactly described by a combination of an infinite number of structural modes. For practical considerations, only a limited number of modes can be con-

Presented as Paper 84-0870 at the AIAA/ASME/ASCE/AHS 25th Structures, Structural Dynamics and Materials Conference, Palm Springs, CA, May 14-16, 1984; received July 1, 1984; revision received April 4, 1985. This paper is declared a work of the U.S. Government and therefore is in the public domain.

*Principal Analyst. Informatics General Corporation. Member AIAA.

†Graduate Student. Presently Associate Engineer Senior, Lockheed Missiles and Space Co., Sunnyvale, CA. Member AIAA.

‡Professor and Dean, School of Engineering. Associate Fellow AIAA.

§Research Scientist. Associate Fellow AIAA.

sidered. All modes that contribute significantly to the dynamic motion of the wing should be included in the analysis. The modal participation depends not only on the geometry and physical properties of the wing but also on the flight conditions. The contributing modes for a wing operating in transonic flow can be entirely different from those for the same wing in subsonic flow. Flutter analyses that compare well with experiment in subsonic flow can deviate substantially as the flow becomes transonic. This was demonstrated in Ref. 4, in which a study of a rectangular wing is reported. Only the fundamental structural modes were considered and inviscid aerodynamics were used. The neglect of viscosity and higher structural modes may have been the cause of the deviation. In this work, effects of modes on flutter speeds were studied in the transonic regime.

To illustrate the effects of viscosity and structural modes on flutter speeds, two wings were studied. The first was an unswept, rectangular wing with a full-span aspect ratio of 4 and an NACA 64A010 airfoil section. This wing has been accepted by AGARD[8] as a standard wing for aerodynamic and aeroelastic research. Also, a typical transport wing with a sweep angle of 25 deg, taper ratio of 0.4, and an MBB-A3 supercritical airfoil was studied. Steady and unsteady aerodynamic results for the rectangular wing were obtained at $M=0.7$, 0.80, 0.85, and 0.90 for the inviscid calculations; at $M=0.80$, 0.85, and 0.90 for the viscous wedge calculations; and at $M=0.80$ and 0.85 for the lag-entrainment calculations. Studies were made at $M=0.85$ for the swept wing. In this analysis, all the aerodynamic computations were made using the recently improved version of the code ATRAN3S, which has been verified with wind tunnel results.[9] The version of the code has better coordinate transformations and viscous correction methods. Viscous correction methods used in ATRAN3S are verified with experiments.[6,7] A three-dimensional, assumed mode flutter analysis was used to determine flutter boundaries. The equations of motion were solved using the *U-g* method.[10-12]

Unsteady Transonic Aerodynamic Equations of Motion

The inviscid, three-dimensional, unsteady, transonic, small-disturbance potential equation as described in Ref. 7 is

$$\frac{\partial}{\partial t}(A\phi_t + B\phi_x) = \frac{\partial}{\partial x}(E\phi_x + F\phi_x^2 + G\phi_y^2) + \frac{\partial}{\partial y}(\phi_y + H\phi_x\phi_y) + \frac{\partial}{\partial z}(\phi_z) \tag{1}$$

where ϕ is the perturbation velocity potential function and

$$A = M_\infty^2 k^2$$

$$B = 2M_\infty k$$

$$E = 1 - M_\infty^2$$

$$F = -(\tfrac{1}{2})(\gamma+1)M_\infty^2$$

$$G = (\tfrac{1}{2})(\gamma-3)M_\infty^2$$

$$H = -(\gamma-1)M_\infty^2$$

For inviscid calculations the flow-tangency condition is

$$\phi_z^{\pm} = f_x^{\pm} + kf_t^{\pm} \tag{2}$$

on $z=0^{\pm}$ for $x_{LE} \le x \le x_{TE}$, $0 \le y \le y_{tip}$ where f is the airfoil ordinate, and k is the reduced frequency based on the full chord. The jump across the trailing-edge vortex is

$$[\phi_z] = 0 \text{ and } [\phi_x + k\phi_t] = 0 \tag{3}$$

on $z=0^{\pm}$ for $x > x_{TE}$, $0 \le y \le y_{tip}$. The brackets [ ] indicate a jump in the parameter across the wake. These are the boundary conditions that are modified to include the viscous effects. Transformation equations to map a swept-tapered planform in the physical domain into a rectangle in the Cartesian domain are given in detail in Ref. 9.

When performing transonic aerodynamic calculations, viscous effects often play an important role. Besides altering the shock strength and location, boundary-layer displacements cause camber modifications to the airfoil surface and displacement and camber effects near the wake. The first, and simplest, of the two viscous techniques used in ATRAN3S is the viscous wedge method. Previous studies have shown that the shock/boundary-layer interaction can be modeled by placing a wedge-nosed ramp on the airfoil surface just downstream of the shock found from the inviscid calculations. The ramp slope depends on the shock strength and is calculated for each time step. The change in the surface geometry is described by the modified small-disturbance tangency condition,

$$\phi_z^{\pm} = f_x^{\pm} + kf_t^{\pm} + (f_R^{\pm})_x \text{ on } z=0^{\pm} \text{ for } x_{LE} \le x \le x_{TE},\ 0 \le y \le y_{tip} \tag{4}$$

This viscous wedge method is two-dimensional and is applied to the wing at each spanwise coordinate. Details of computing the ramp slope f_R can be found in Ref. 7. A two-dimensional shock profile was used to determine the placement of the wedge in this study, as opposed to the three-dimensional shock profile discussed in Ref. 7. This change was made to help reduce oscillations in the pressures obtained when using the viscous methods.

For some calculations, the wedge model alone is sufficient for accurate determination of the unsteady viscous pressure distributions. For other calculations, however, a more exact analysis is required to model the viscous effects. To do this, the wedge correction is used along with a set of integral boundary-layer equations, called the lag-entrainment equations,[7] to perform viscous calculations downstream of the shock wave, including the downstream wake. These equations are governed by three first-order ordinary differential equations.[7] This method assumes that viscous regions are small relative to the wing or wake thickness. The modification to the small-disturbance surface tangency condition for the lag-entrainment method is

$$\phi_z^{\pm} = f_x^{\pm} + (k_i^{\pm}) + (F_1 + F_2\phi_{xx})^{\pm} \text{ on } z=0^{\pm} \text{ for } x_{LE} \le x \le x_{TE},\ 0 \le y \le y_{tip} \tag{5}$$

The downstream wake conditions are defined by

$$[\phi_z] = [F_1 + F_2\phi_{xx}] \text{ on } z=0 \text{ for } x > x_{TE},\ 0 \le y \le y_{tip} \tag{6}$$

and F_1 and F_2 are obtained by solving the lag-entrainment equations.[7] The time step must be sufficiently small to ensure that the method is stable, as has been demonstrated in two dimensions.[6] These viscous methods were derived for steady-state computations and incorporated into the unsteady equations of motion in a quasi-steady fashion. The aerodynamic pressure data required at any time step for viscous correction equations are taken from the previous time step.

To solve the governing equations numerically, the flowfield is discretized in the computational domain by using a three-

dimensional Cartesian grid.[2] The grid used for both wings in this study contained 64 points in the streamwise direction, 20 points in the spanwise direction, and 40 points in the vertical direction. The wing was discretized into 39 points in the streamwise direction and 13 points in the spanwise direction. The displacement of each grid point on the wing was prescribed for each mode. The analysis was uncoupled, requiring one run of the transonic code for each mode of motion of the wing.

Procedure

The generation of the aerodynamic data is performed separately from the aeroelastic analysis. First, ATRAN3S is used to generate the steady and unsteady aerodynamic data by prescribing the wing motion. These data are then input into the aeroelastic equations of motion to solve for the flutter speed. An alternative procedure would be to solve both sets of equations in a coupled manner. This procedure is also possible with ATRAN3S, and an example calculation is described in Ref. 13. Using the former method, the unsteady solutions were obtained by forcing the wing to oscillate sinusoidally as the aerodynamic equation of motion was integrated in time. To obtain a steady solution, the amplitude of motion was set to zero. The unsteady viscous calculations were restarted from corresponding steady-state solutions. For unsteady calculations, three cycles of motion were sufficient for the transients to die out and for a periodic solution to be obtained. For most inviscid calculations, 360 time steps per cycle were used. However, for a Mach number of 0.70 and a reduced frequency k of 0.1, 720 time steps per cycle were required. Viscous calculations typically required 720 time steps per cycle for the wedge calculations and 2160 time steps per cycle for the lag-entrainment calculations. Unsteady aerodynamic coefficients, based on the third cycle, were used to compute flutter boundaries for inviscid and viscous calculations.

Solutions obtained using the original viscous corrections incorporated into XTRAN3S[2] contained high-frequency oscillations in the unsteady air loads. An investigation into this problem determined that the shock sweep angles computed for the viscous wedge[7] corrections did not change smoothly across the span, but instead jittered in some span regions, as well as with time step, at some span locations. Also, it was determined that the use of these shock sweep angles to determine the shock location was not consistent with the method of locating the shock wave for use in the type-dependent differencing that is employed in the inviscid calculations. To correct this inconsistency, the shock location at each span station was determined by only using flowfield values along that span station. This new method of determining the shock location was then used to place the viscous wedge on that span section. Figure 1 shows the unsteady upper-surface pressure across the chord at the 60% semispan station for both the original method and the new method used in this study. The four curves shown represent the pressures for four consecutive time steps in the third cycle of motion. The large fluctuations in the pressure profile at the shock location are eliminated when the new method is used. Even with this improvement, however, high-frequency oscillations in the lift still remain when the viscous corrections are used. Most of these oscillations can be eliminated by using 2880 time steps per cycle. It is known that oscillations are also induced by the shock crossing a mesh point. The use of a finer mesh and other possible solutions are currently under investigation.

A three-dimensional U-g-type flutter analysis has been employed to compute flutter boundaries. A Rayleigh-Ritz procedure was used in which a finite number of bending and torsion mode shapes were assumed to describe the modal motion of the wing at flutter. For this analysis, the first two bending and first two torsion modes were considered. The unsteady aerodynamic forces generated by the deflection of the wing have to be computed separately for each structural mode of motion. Thus, the cost of determining flutter boundaries is a direct multiple of the number of structural modes considered

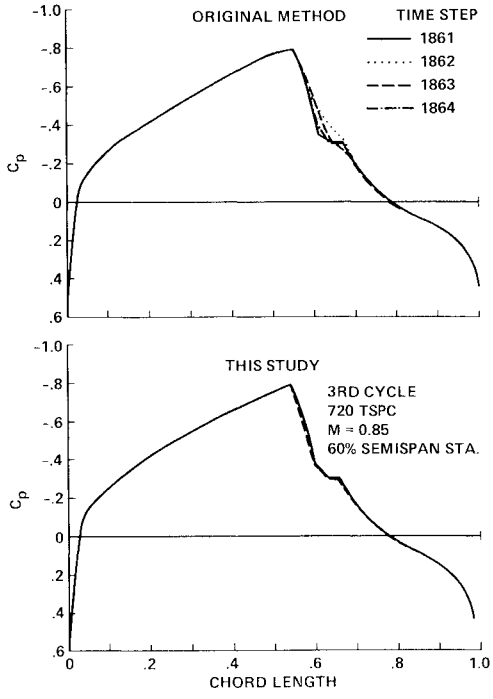

Fig. 1 Comparison of the original viscous wedge method using shock sweep angles and the method used in this study.

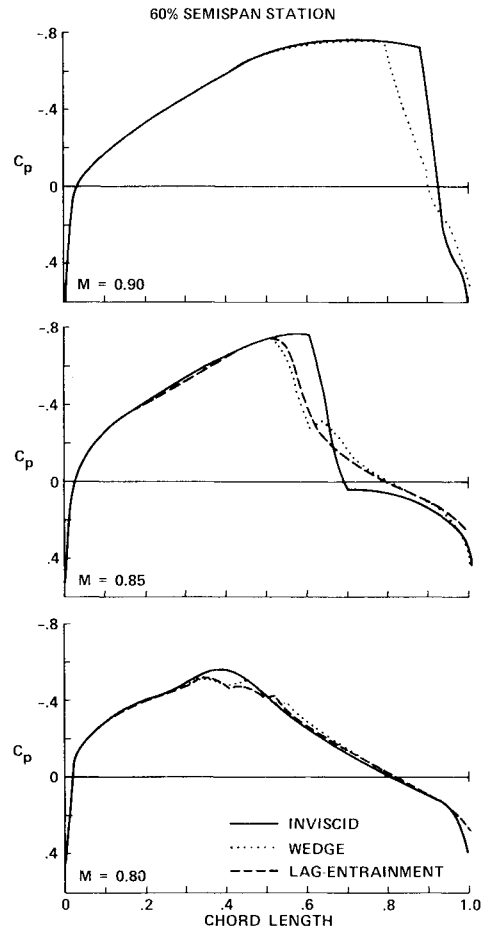

Fig. 2 Rectangular wing steady pressure shown for three Mach numbers and the inviscid and viscous methods at 60% semispan station and $\alpha = 0$.

in the analysis. Because of the cost of computing three-dimensional, unsteady, transonic aerodynamic coefficients, it is not practical to experiment with a large number of structural modes to determine which ones will play a significant role. The geometry of the structure and the boundary conditions applicable to the problem should be carefully considered. Using only the modes significant to the problem will greatly reduce the cost and time required to obtain a solution. In this study, the first two bending and torsion modes were chosen to describe the motion of the low-aspect-ratio, rectangular, cantilever wing. Previous studies have shown that the fundamental modes are sufficient to determine the flutter speed of a rectangular wing in subsonic flow. For comparison, the first two bending and torsion modes were also used for the swept wing. It may be, however, that even higher modes would be significant for this wing owing to its more complex geometry. The deflections caused by the natural mode shapes of the wing were calculated at 39 streamwise points, for each of the 13 span stations, and input into ATRAN3S. The code was run for three complete cycles of motion, and the Fourier coefficients from the third cycle were used to perform the aeroelastic calculations. For the rectangular wing, unsteady calculations were made for four modes at four different Mach numbers and from three to six reduced frequencies for each Mach number. Also the inviscid and the two viscous methods were considered, requiring 168 separate runs of the transonic code. Although only limited results were computed for the swept wing, another 36 runs of the code were required. The inviscid calculations required 500 s of computing time on the Cray X-MP. The wedge and lag-entrainment methods required 1100 and 3300 s, respectively.

Results

Rectangular Wing with NACA 64A010 Airfoil

One of the two wings considered in this study was the AGARD rectangular wing with an aspect ratio of 4 and a NACA 64A010 airfoil cross section. Aerodynamic and flutter results were computed for the rectangular wing at $M=0.8$ and at zero angle of attack, which is one of the AGARD suggested flow conditions.[8] In addition, calculations for the same wing were made at $M=0.70$, $M=0.85$, and $M=0.90$ to determine the effects of Mach number on three-dimensional aeroelastic calculations. First, steady-state pressure distributions were obtained for the inviscid, wedge, and lag-entrainment methods. The steady wedge calculations were restarted from the steady inviscid solution and the steady lag-entrainment calculations were restarted from the steady wedge solution, following the procedure given in Ref. 7. The steady flow became fully developed in 1000 time steps. Figure 2 shows the steady pressure distribution for the three methods at the 60% semispan station and at the three Mach numbers. The code diverged when the lag-entrainment method was used at $M=0.90$, so no results were obtained for those conditions. The forward displacement of the shock and reduction in strength are characteristic of viscous flow. These trends are consistent with those shown in two dimensions for the same airfoil. It can be seen that the lag-entrainment method shows no deviation from the wedge for this particular wing.

The first and second bending and first and second torsion natural modes, shown in Fig. 3, were selected to model accurately the motion of the wing to obtain unsteady aerodynamic coefficients. Calculations were made at reduced frequencies, based on full chord, from 0.1 to 0.6. The maximum deflections were 3.44 deg for the torsion modes and 10% of the chord for the bending modes. The wing was constrained to pitch about the midchord. Figure 4 shows the magnitude of the first harmonic component of the time-dependent, unsteady local lift coefficient and the corresponding phase angle vs span for the rectangular wing at three Mach numbers. Results are shown for inviscid and for both the wedge and lag-entrainment viscous correction methods for the first torsion mode at a reduced frequency of 0.4. As expected from two-dimensional studies,[6] the lift coefficients obtained by the viscous methods are lower than those calculated using the inviscid method; however, the magnitude of the lift using the wedge correction shows little change over the inviscid method. The phase angles show a significant change for both viscous methods.

As mentioned earlier, the flutter boundaries were determined using a three-dimensional *U-g* method. Flutter speeds in this paper are nondimensionalized by dividing flutter speed by the product of the semiroot chord and the circular frequency of the first torsional mode. Of primary interest in this study were the aeroelastic characteristics of the rectangular wing related to the effects of the structural modes and flow viscosity. Four combinations of the first two pure bending and torsion modes were considered. First, only the first bending and first torsion modes were included. Then the second modes of each type were added individually. Finally, all four modes, namely, first bending, second bending, first torsion, and second torsion, were all included in the solution. For the modal analysis, the wing was configured so that the elastic axis and center of mass were located at 45% and 60% of the root chord, respectively, aft of the leading edge. The wing section to air mass density ratio μ was assumed to be 200. The first bending (ω_{h1}), second bending (ω_{h2}), first torsion ($\omega_{\alpha 1}$), and

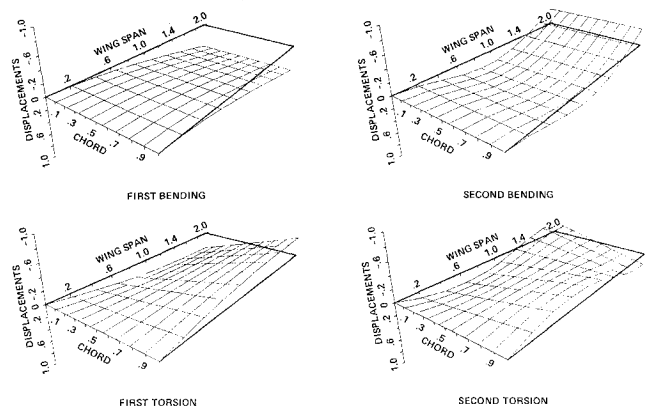

Fig. 3 Rectangular wing natural mode shapes.

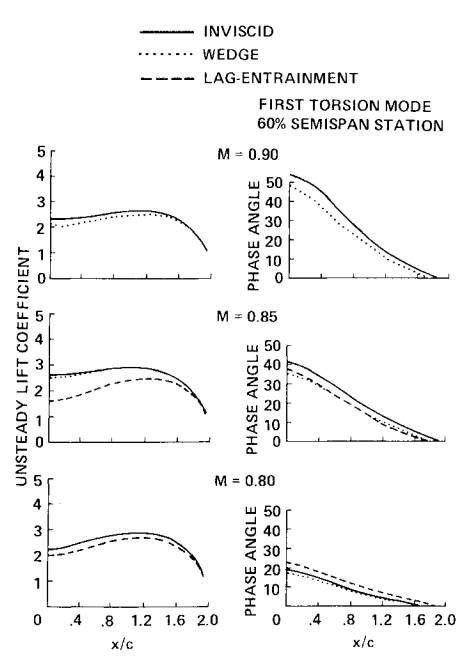

Fig. 4 Magnitude of unsteady lift and corresponding phase angle vs span for the inviscid and viscous methods.

Table 1 Flutter speeds for various modal combinations: rectangular wing

	$M=0.70$	$M=0.80$			$M=0.85$			$M=0.90$	
Modes	Inviscid	Inviscid	Wedge	Lag entrainment	Inviscid	Wedge	Lag entrainment	Inviscid	Wedge
First bending, first torsion	3.2511	1.8810	1.9556	1.990	1.0503	1.1542	1.1283	1.1934	1.2956
First and second bending, first torsion	3.2910	1.8810	1.9557	1.991	1.0503	1.1541	1.1282	1.1933	1.2956
First bending, first and second torsion	3.2524	1.8816	1.9561	1.995	1.0504	1.1546	1.1283	1.1942	1.2962
First and second bending, first and second torsion	3.2897	1.8816	1.9562	1.995	1.0506	1.1549	1.1285	1.1941	1.2964

Note: 1) Elastic axis is located 45% chord from the leading edge. 2) Mass center is located 55% chord from the leading edge. 3) Wing section to air density ratio (μ) = 200. 4) Modal frequencies of first bending (ω_{h1}), second bending (ω_{h2}), first torsion ($\omega_{\alpha 1}$), and second torsion ($\omega_{\alpha 2}$) are 25, 143, 87, and 261 rad/s, respectively.

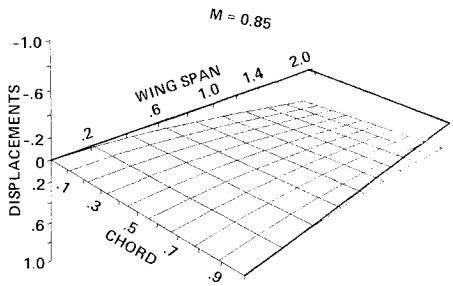

Fig. 5 The shape of the rectangular wing at flutter is composed of the first bending and torsion modes.

second torsion ($\omega_{\alpha 2}$) frequencies were assumed to be 25, 143, 87, and 261 rad/s, respectively. For the rectangular wing, the first bending and torsion modes were sufficient to determine the flutter speed (Table 1). The flutter frequency in all cases is very close to the first bending frequency, which explains the dominance of the first bending mode. Figure 5 shows the deflection of the wing at flutter. It closely resembles the first bending mode. Many of the aeroelastic parameters were varied to see if any effect of the higher modes could be obtained; little to no effect was seen. Only when very unrealistic values were used was an appreciable effect of modes noticed.

The effect of flow viscosity is an important factor to consider when computing the flutter boundaries of a wing in transonic flow. Viscosity can have a noticeable effect on the aerodynamic forces acting on the wing and, hence, on the flutter boundaries. Previously, only inviscid calculations had been made on wings. Viscous calculations were made at three Mach numbers, $M=0.80$, $M=0.85$, and $M=0.90$. For each Mach number, aerodynamic coefficients were calculated over a range of reduced frequencies from 0.1 to 0.6 and for the same four structural modes discussed earlier. The wedge and lag-entrainment viscous methods were used. At $M=0.85$, the flow is transonic and the shock is well defined. Figure 6 shows the sectional magnitude and corresponding phase angle of the lift coefficient vs the reduced frequency for the inviscid method and for two viscous methods. Sectional parameters are shown for span station at the 60% semispan location. This figure shows that the lift coefficients calculated with viscous corrections included are slightly below the inviscid calculations. This is the trend that was anticipated because it corresponds to trends shown for two-dimensional airfoils. This small reduction in force, coupled with significant changes in the phase angles, contributes to the higher flutter speeds shown for the viscous methods in Fig. 7 and Table 1. A well-defined transonic dip can be seen in Fig. 7, with the lowest flutter speed occurring between $M=0.85$ and $M=0.90$. Flutter speed drops by a factor of 3.0 from subsonic ($M=0.70$) to high transonic

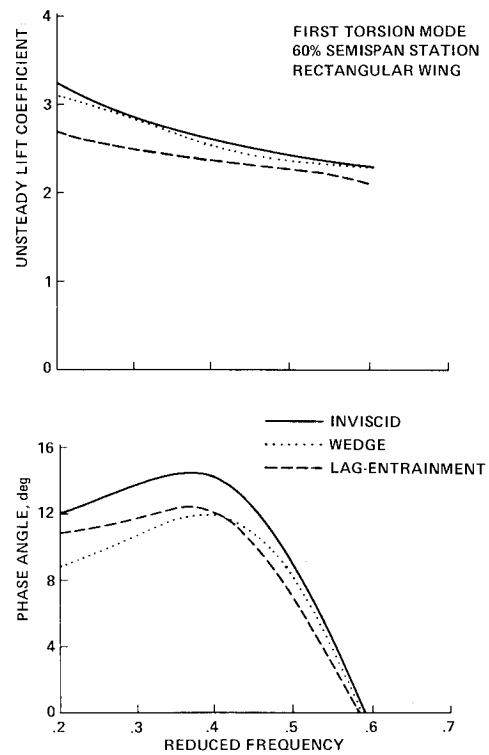

Fig. 6 Magnitude of unsteady lift and corresponding phase angle vs reduced frequency for the inviscid and viscous methods.

($M=0.90$) because of the changes in aerodynamic forces that can be observed in Fig. 2 (subsonic steady pressure for $M=0.70$ is not shown in the figure). Inclusion of the viscous corrections resulted in about a 10% increase in flutter speed. The increase in flutter speed is a direct result of the viscous corrections causing a reduction in the magnitude of the lift coefficient. A higher flutter speed may not always follow from a reduction in magnitude of the lift because the change in phase angle must also be considered when one is trying to anticipate flutter trends. The wedge correction required little more computational effort than the inviscid method, but yielded an increase in flutter speed, as is depicted in Fig. 7. The lag-entrainment method, on the other hand, required 6 to 8 times the computing time to obtain a converged, stabilized solution. The results obtained using the lag-entrainment method were about the same as the wedge correction provided. It is noted that the wedge calculations were performed at 720 time steps per cycle, and the lag-entrainment calculations were performed at 2160 time steps per cycle.

Table 2 Flutter speeds for various modal combinations: swept wing, $M=0.85$

Modes	Inviscid	Wedge	Lag entrainment
First bending, first torsion	2.1237	2.8507	2.2066
First and second bending, first torsion	2.1240	2.8504	2.2057
First bending, first and second torsion	2.0666	2.9511	2.1856
First and second bending, first and second torsion	2.0670	2.9502	2.1850

Note: 1) Elastic axis is located 45% chord from the leading edge. 2) Mass center is located at 60% chord from leading edge. 3) Wing section to mass ratio (μ) = 200. 4) Modal frequencies of first bending (ω_{h1}), second bending (ω_{h2}), first torsion ($\omega_{\alpha 1}$) and second torsion ($\omega_{\alpha 2}$) are 25, 250, 30, and 40 rad/s, respectively.

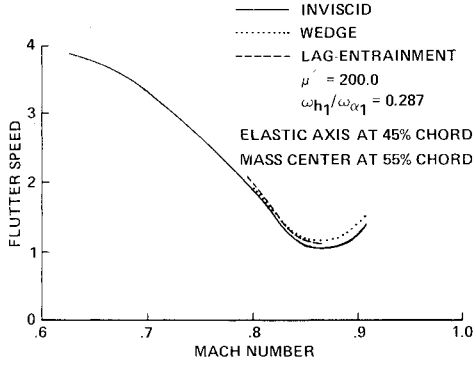

Fig. 7 Effect of Mach number and viscosity on flutter speed.

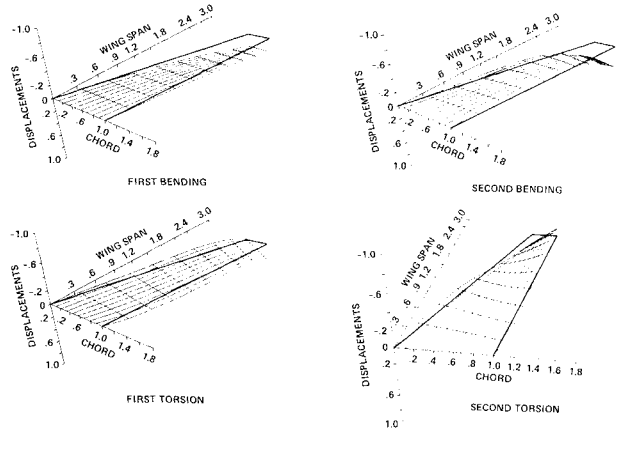

Fig. 8 Swept wing natural mode shapes.

Swept Wing with MBB-A3 Airfoil

This swept wing was chosen to represent a typical transport-type wing. It has a full-span aspect ratio of 8, a taper ratio of 0.4, leading-edge sweep angle of 25 deg, and an MBB-A3 supercritical airfoil section. Because of the complex geometry, the computing time required for this case was twice that required for similar calculations on the rectangular wing. Aerodynamic and flutter calculations were made inviscidly, as well as by using the wedge and lag-entrainment viscous corrections at a Mach number of $M=0.85$. As was done for the rectangular wing, steady-state data were computed, and then the

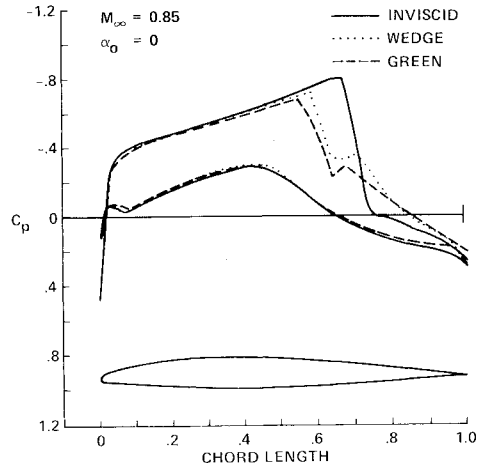

Fig. 9 Swept wing steady pressure for the inviscid and viscous methods at 60% semispan and $\alpha=0$.

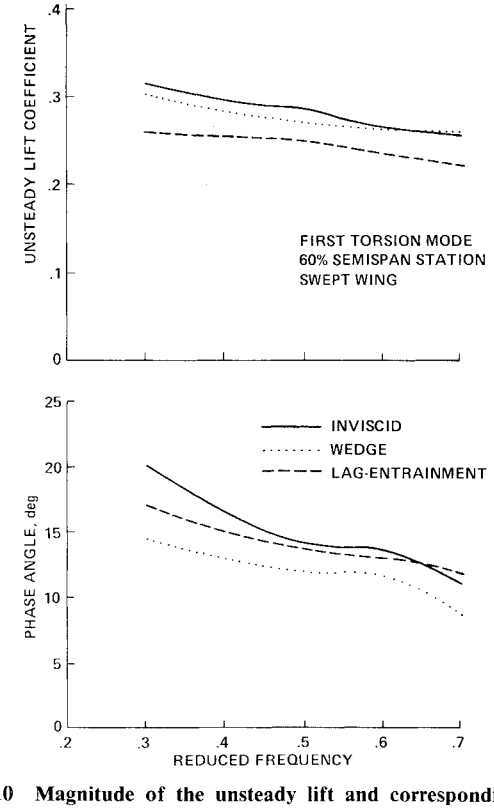

Fig. 10 Magnitude of the unsteady lift and corresponding phase angle vs reduced frequency for the inviscid and viscous methods.

unsteady runs were restarted from the corresponding steady-state data files.

The first bending, first torsion, second bending, and second torsion modes were incorporated into the flutter analysis of the swept wing (Fig. 8). Again the deflections of the wing were computed for each mode at 507 wing locations to describe the deflection shapes in the transonic code. It can be seen that the modes, despite the sweep and taper, are very similar to the corresponding modes for a cantilever beam. To obtain a converged inviscid solution, 720 time steps per cycle were required; 1440 and 2880 time steps per cycle were required for the viscous wedge and lag-entrainment methods, respectively. Calculations were made at $k=0.4$, 0.5, 0.6, and 0.7 for all three methods. The steady pressure across the chord, at the 60% semispan location is shown in Fig. 9 for all three methods and for both the upper and lower surfaces. The viscous wedge shows a shock that has moved forward of the inviscid shock

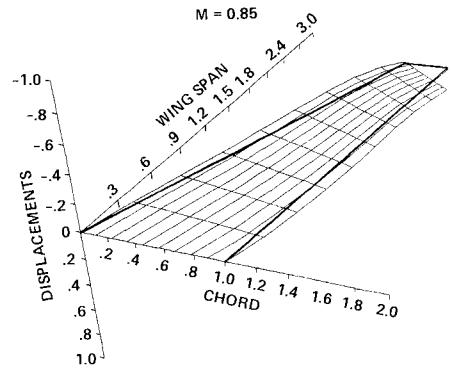

Fig. 11 The shape of the swept wing at flutter is composed of the first bending and the first and second torsion modes.

and is much weaker. The lag-entrainment correction causes the shock to move still farther forward. For this wing and airfoil section, the lag-entrainment method does show a significant change from the viscous wedge method.

Figure 10 shows the magnitude and corresponding phase angle of the lift coefficient plotted vs reduced frequency. The same trend is shown here as was shown for the rectangular wing. The magnitude of the inviscid lift is greater than the viscous wedge lift, although only slightly, which is even greater than the lift calculated using the viscous lag-entrainment method.

Flutter calculations were performed on this wing at $M=0.85$; the results are shown in Table 2. For this case the elastic axis and mass center were located at 40% and 60% chord, respectively, from the leading edge. The mass ratio μ was assumed as 200, based on the root chord. Modal frequencies ω_{h1}, ω_{h2}, $\omega_{\alpha 1}$, and $\omega_{\alpha 2}$ were assumed as 25, 250, 30, and 60 rad/s, respectively. Here again, the primary modes dominate the flutter solution. For this wing, however, the second torsion mode does cause a noticeable change in the flutter speed. When the second bending mode was added to the primary modes, only an insignificant change in the flutter speed was noted, but when the second torsion mode was added, the flutter speed decreased by about 5%. It was expected that the torsion modes would play an important role in this analysis because of the sweep of the wing. The first two torsion modes can be seen along with the first bending mode in Fig. 11.

A 26% increase in flutter speed was observed when the viscous wedge method was used. On the other hand, when aerodynamics that included the lag-entrainment method were input into the equations of motion, the flutter speed showed only a slight increase over that of the inviscid flutter solution. It can be seen in Fig. 10 that the change in phase angle from the inviscid solution is much greater for the wedge calculations than for the lag-entrainment calculations.

Conclusions

This study was performed to aid in the verification of the three-dimensional, unsteady, transonic, aerodynamic computer code ATRAN3S. Viscous calculations were made using the viscous wedge and lag-entrainment viscous correction methods. Flutter analyses were performed on two wings, and the effects of viscosity and modes were studied. From this work several conclusions may be drawn.

The results discussed in this paper indicate that two-dimensional viscous methods may be applied to three-dimensional flows over wings. Viscous solutions produce higher flutter speeds than inviscid solutions. This is due to the fact that viscous effects decrease the lifting forces. From the analysis made on the single-degree-of-freedom system, it is observed that the increasing lifting forces decrease flutter speed. The current viscous methods tend to induce oscillations into the solution that do not occur in inviscid calculations. The implementation of a two-dimensional shock profile, used to place the wedge, helped to reduce these oscillations. Further research is required to improve the implementation of the viscous correction methods into ATRAN3S, as well as other inviscid codes. For the rectangular wing, the lag-entrainment method required three times as much computational time as the wedge method, but the two solutions deviated only slightly.

It is important to know which structural modes play a contributing role in a transonic flutter solution. Computing costs are directly proportional to the number of modes considered. For the rectangular wing with a low aspect ratio, the primary modes proved sufficient to determine the flutter speed accurately. For swept tapered wings, higher bending modes may not be as significant as higher torsion modes. At least the first two torsion modes must be considered when performing an aeroelastic analysis on a swept clean wing.

References

[1]Traci, R. M., Albano, E. D., and Farr, J. L., "Small Disturbance Transonic Flows about Oscillating Airfoils and Planar Wings," AFFDL-TR-75-100, Air Force Flight Dynamics Laboratory, June 1975.

[2]Borland, C. J., Rizzetta, D. P., and Yoshihara, H., "Numerical Solution of Three-Dimensional Unsteady Transonic Flow over Swept Wings," AIAA Paper 80-1369, July 1980.

[3]Borland, C. J. and Rizzetta, D. P., "Nonlinear Transonic Flutter Analysis," *AIAA Journal*, Vol. 20, Nov. 1982, pp. 1606-1615.

[4]Guruswamy, P. and Goorjian, P. M., "Comparison between Computational and Experimental Data in Unsteady Three-Dimensional Transonic Aerodynamics, Including Aeroelastic Applications," AIAA/ASCE/ASME/AHS Structures, Structural Dynamics, and Materials Conference, New Orleans, LA, May 1982.

[5]Myers, M. R., Guruswamy, P., and Goorjian, P. M., "Flutter Analysis of a Transport Wing Using XTRAN3S," AIAA/ASCE/ASME/AHS Structures, Structural Dynamics, and Materials Conference, Lake Tahoe, NV, May 1983.

[6]Guruswamy, P. and Goorjian, P. M., "Effects of Viscosity on Transonic Aerodynamics and Aeroelastic Characteristics of Oscillating Airfoils," AIAA/ASCE/ASME/AHS Structures, Structural Dynamics, and Materials Conference, Lake Tahoe, NV, May 1983.

[7]Rizzetta, D. P. and Borland, C. J., "Numerical Solution of Three Dimensional Unsteady Transonic Flow over Wings Including Inviscid/Viscous Interaction," AIAA 20th Aerospace Sciences Meeting, Orlando, FL, Jan. 1982.

[8]Bland, S. R., "AGARD Three Dimensional Aeroelastic Configurations," NASA Langley Research Center, Hampton, VA, AGARD-AR-167, March 1982.

[9]Guruswamy, P. and Goorjian, P. M., "Development and Application of XTRAN3S—Ames," presented at the Computational Fluid Dynamics Users Workshop, University of Tennessee Space Institute, Tullahoma, TN, March 1984.

[10]Yang, T. Y., Guruswamy, P., Stritz, A. G., and Olsen, J. J., "Flutter Analysis of a NACA 64A006 Airfoil in Small Disturbance Transonic Flow," *Journal of Aircraft*, Vol. 17, April 1980, pp. 225-232.

[11]Bisplinghoff, R. L., Ashley, H., and Halfman, R. L., *Aeroelasticity*, Addison-Wesley Publishing Company, Menlo Park, CA, 1957.

[12]Fung, Y. C., *Theory of Aeroelasticity*, Dover Publications, Inc., New York, 1969.

[13]Guruswamy, P., Ide, H., Goorjian, P. M., and Miller, G. D., "Transonic Aeroelastic Analysis of the B-1 Wing," AIAA Structural Dynamics Conference, Orlando, FL, April 1985.